To cite this article: NIE Y Z, OUYANG W, LI G Q, et al. Simulation study on hydrodynamic performance of podded propulsor for curise ship[J/OL]. Chinese Journal of Ship Research, 2022, 17(3). http://www.ship-research.com/en/article/doi/10.19693/j.issn.1673-3185.02491.

DOI: 10.19693/j.issn.1673-3185. 02491

Simulation study on hydrodynamic performance of podded propulsor for cruise ship

NIE Yuanzhe[1], *OUYANG Wu*[1,2], *LI Gaoqiang*[1], *ZHANG Cong*[1,2], *ZHOU Xincong*[1,2]

1 School of Transportation and Logistics Engineering, Wuhan University of Technology, Wuhan 430063, China

2 Reliability Engineering Institute, National Engineering Research Center Water Transport Safety, Wuhan 430063, China

Abstract: [**Objective**] Aiming at the mapping relationship between combined hydraulic components and performance, the hydrodynamic performance prediction method of a podded propulsor for a cruise ship based on Reynolds-averaged Navier-Stokes (RANS) is studied. [**Methods**] Taking a scale model of a podded propulsor as the research object, the open water performance test of the propulsor is carried out in a deepwater towing tank, and the accuracy of the prediction method is verified. The effects of pod geometry, disk ratio, and blade number on the hydrodynamic performance of the podded propulsor are simulated and analyzed. [**Results**] The results show that the geometry of the pod has little effect on the open water performance of the propulsor. Increasing the disk ratio of the propeller causes the thrust coefficient and open water efficiency to first increase and then decrease, while the torque coefficient only increases within a certain range. Increasing the number of propeller blades will first increase and then decrease the open water performance of the propulsor, and the number of propeller blades has little effect on the open water efficiency of the podded propulsor under low advance coefficient. [**Conclusion**] The results of this study can provide reference value for the optimal design of cruise ship podded propulsors.

Key words: cruise ship; podded propulsor; hydrodynamic performance; computational fluid dynamics (CFD); optimization design

CLC number: U664.3; U661.71

0 Introduction

The podded propulsor, as an integrated electric propulsor, embeds the propulsion motor into the pod and is installed under the hull through the column. The propeller is directly connected to the motor output shaft, and the 360° full rotation can be achieved after the propeller is connected to the rotary device. This electric direct-drive mode enables transmission-free energy conversion and the integration of propulsion and steering. Compared with the traditional diesel-powered mechanical propulsion system, the electric podded propulsion system has salient advantages, such as high power density, small overall space occupation, low vibration and noise, and being green and energy-saving [1]. For high-performance ships, the podded propulsor can also enable vector propulsion, thereby improving the maneuverability and safety of the ships. World-renowned podded propulsor products mainly include Azipod, SSP, Mermaid, and Dolphin [2]. Specifically, the propulsion power of ABB's Azipod, Compact Azipod, and CRP Azi-pod series products cover 0.4−90 MW. At present, the podded propulsor

Received: 2021 − 08 − 23 **Accepted**: 2022 − 10 − 27

Supported by: High Technology Ship Scientific Research Project of the Ministry of Industry and Information Technology of China (MC-201917-C09)

Authors: NIE Yuanzhe, male, born in 1999, master's degree candidate. Research interest: hydrodynamics of podded propulsor. E-mail: 2945277154@qq.com

OUYANG Wu, male, born in 1987, Ph.D., professor. Research interest: green and efficient propulsion technology. E-mail: ouyangw@whut.edu.cn

***Corresponding author**: OUYANG Wu

has become an alternative propulsion scheme for some types of ships, such as icebreakers, research ships, luxury cruise ships, and offshore platforms.

The combined hydraulic components of a podded propulsor include the propeller, pod, column, and other appendages, and they jointly determine the hydrodynamic performance of the propulsor. Nevertheless, the interaction mechanism between hydraulic components and the fluid is more complicated than that between a simple propeller and the fluid. At present, the research methods for hydrodynamics mainly include experimental methods and numerical calculation methods. In terms of experiments, Islam et al. [3] conducted an experimental study of the open water propulsion performance of the tractor-type podded propulsor under azimuthing conditions and measured the thrust, torque, and rotational speed of the propulsor and the forces and torques in three orthogonal directions. He et al. [4] experimentally investigated the hydrodynamic performance of a tandem-type podded propulsor under different azimuthing angles. Islam et al. [5] took an icebreaker with a tandem-type podded propulsor as an example to study the performance of the propulsor under open water conditions and different ice conditions. Zhao et al. [6] employed particle image velocimetry to measure the flow field characteristics of an L-shaped podded propulsor under different working conditions and studied the interaction laws among the propeller, the pod body, and the strut under different advance coefficients and azimuthing angles. Feng et al. [7] conducted a self-propulsion test on a luxury cruise ship model with pod propulsion and studied the changes in propeller speed and torque under the action of regular and irregular waves. In addition, according to research, the open water performance data of the ducts and propellers of the podded propulsor could be more accurately measured by a circulating water channel or towing tank after a dynamometer is installed.

Regarding numerical calculation, Cheng et al. [8] built an ideal model based on the potential flow theory back in the 1980s and simulated the steady hydrodynamic performance of the propeller, which was further used to predict the performance of the pod propulsion ship. After that, Taskar et al. [9], Bal et al. [10], and Ye et al. [11] all used the potential flow method to study the hydrodynamic performance of podded propulsors. As computer performance continuously improves, researchers have begun to utilize viscous flow methods for numerical calculation. For example, Shamsi et al. [12] and Zhu et al. [13] calculated the hydrodynamic performance of podded propulsors with Reynolds-averaged Navier-Stokes (RANS) equations and verified the accuracy of the calculation results experimentally. Zhang et al. [14] resorted to the improved delayed-detached eddy simulation (IDDES) method to study the interaction between the front and rear propellers of a podded propulsor with hybrid contra-rotating propellers (CRPs) numerically, with the focus laid on the details of the thrust, torque, and flow field. Yao et al. [15] numerically simulated the open water performance of a three-dimensional full-scale bare propeller and a podded propulsor according to the viscosity theory with sliding mesh technology.

Although scholars in China and abroad have carried out a lot of research on predicting and testing the hydrodynamic performance of the podded propulsor, a clear mapping relationship between these combined hydraulic components and their hydrodynamic performance remains to be established. Consequently, the forward design theory and optimization method for the hydrodynamic performance of podded propulsors are still a difficult problem that seriously restricts China's independent research and development ability for large podded propulsors. Therefore, this paper takes the podded propulsor of a luxury cruise ship as the object and intends to investigate the influences of different structural parameters on the performance of the propulsor through simulation analysis and experimental verification of the hydrodynamic performance of the podded propulsor in light of the computational fluid dynamics (CFD) theory to provide a reference for the design of the podded propulsor of cruise ships.

1 Fundamentals of CFD simulation of podded propulsor

1.1 Governing equation

The hydrodynamic model of the podded propulsor mainly involves the mass conservation equation (Eq. (1)) and the momentum conservation equation (Eq. (2)) of fluid:

$$\frac{\partial \rho}{\partial t}+\frac{\partial(\rho u_1)}{\partial x}+\frac{\partial(\rho u_2)}{\partial y}+\frac{\partial(\rho u_3)}{\partial z}=0 \tag{1}$$

$$\oint_A (w\cdot \boldsymbol{n})\rho w \mathrm{d}A=\int_\tau \rho F \mathrm{d}\tau+\oint_A p_\mathrm{n}\mathrm{d}A \tag{2}$$

where ρ is the density; t is the time; u_1, u_2, u_3 are the components of the velocity vector in x, y, z directions, respectively; A is the area of the control sur-

face; w is the fluid velocity; $\boldsymbol{n}$ is the outer normal unit vector on the control surface element; τ is the volume of the control body; F is the mass force acting on the unit mass of fluid on the control body; p_n is the fluid stress.

When the flow passes through the podded propulsor, the flow is generally turbulent, so the basic equation of turbulence needs to be added. Since the turbulent flow can be regarded as the superposition of a time-averaged flow and an instantaneous pulsating flow, the RANS equation can be obtained by averaging the Navier-Stokes (N-S) equation in the time domain:

$$\frac{\partial \rho}{\partial t}+\frac{\partial(\rho u_i)}{\partial x_i}=0 \tag{3}$$

$$\frac{\partial(\rho u_i)}{\partial t}+\frac{\partial(\rho u_i u_j)}{\partial x_j}=-\frac{\partial P}{\partial x_i}+\frac{\partial \tau_{ij}}{\partial x_j}+\frac{\partial(-\rho\overline{u_i' u_j'})}{\partial x_j} \tag{4}$$

where u_i and u_j (i, j = 1, 2, 3) are the components of the velocity vectors in the three coordinate directions; x_i and x_j are the displacements in the three coordinate directions based on the velocity components; P is the pressure; τ_{ij} is the stress tensor component; $-\rho\overline{u_i' u_j'}$ is the Reynolds stress.

1.2 Turbulence model

When the podded propulsor works, its main moving part is the propeller. At present, the SST k-ω turbulence model provides the best overall effect in simulating the hydrodynamic performance of the propeller. Nevertheless, it imposes a higher requirement on the size of the meshes near the wall. In contrast, the standard k-ω model is more robust and provides simple calculations, although it is less accurate [16]. As an improved version of the standard k-ε model, the realizable k-ε model offers excellent performance in rotating flow, boundary layer flow with a large adverse pressure gradient, flow separation, and secondary flow and thus better balances the calculation cost and accuracy. Therefore, this paper resorts to the realizable k-ε turbulence model to solve the equations. The specific form is as follows [17]:

$$\frac{\partial(\rho k)}{\partial t}+\frac{\partial(\rho\varepsilon\bar{u}_i)}{\partial x_i}=\frac{\partial}{\partial x_j}\left[\left(\mu+\frac{\mu_t}{\sigma_\varepsilon}\right)\frac{\partial \varepsilon}{\partial x_j}\right]+\rho C_1 E\varepsilon-\rho C_2\frac{\varepsilon^2}{k+\sqrt{\nu\varepsilon}} \tag{5}$$

$$\frac{\partial(\rho k)}{\partial t}+\frac{\partial(\rho k\overline{u_i})}{\partial x_i}=\frac{\partial}{\partial x_j}\left[\left(\mu+\frac{\mu_t}{\sigma_k}\right)\frac{\partial k}{\partial x_j}\right]+G_k-\rho\varepsilon \tag{6}$$

where k is the turbulent kinetic energy; ε is the dissipation rate of the turbulent kinetic energy; $\bar{u}_i$ is the time-averaged velocity; μ is the fluid dynamic viscosity; μ_t is the turbulent kinematic viscosity; σ_ε is the Prandtl number corresponding to the dissipation rate ε; C_1 and C_2 are empirical parameters; E is the time-averaged strain rate; ν is the fluid kinematic viscosity; σ_k is the Prandtl number corresponding to the turbulent kinetic energy k; G_k is the generation item of the turbulent kinetic energy k caused by the average velocity gradient.

2 Calculation model and experimental verification

2.1 Model of podded propulsor

In this paper, the software STAR-CCM+ is used to simulate the open water performance of the propulsor. The analysis object is a large tractor-type podded propulsor of a luxury cruise ship. Its main components include the propeller, pod, column, and fin. A three-dimensional reduced scale model of the propulsor (Fig. 1) is built by reducing the size of the propulsor (the difference between the Reynolds numbers of the actual object and the reduced scale model is two orders of magnitude) and retaining the components and structure of the propulsor. The main parameters are shown in Table 1, where R is the radius of the propeller.

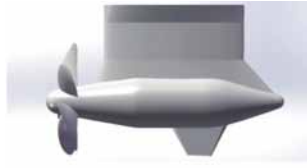

(a) Front view

(b) Rear view

(c) Left view

(c) Right view

Fig. 1 Multi-angle views of reduced scale model of podded propulsor

Table 1 Main parameters of podded propulsor

Parameter	Value
Propeller diameter D/mm	200
Propeller blade number Z	5
Disk ratio	0.67
Pitch ratio at 0.7R	1.15
Chord length at 0.75R/mm	63.2
Blade thickness at 0.75R/mm	3.24
Rotation direction	Right-handed
Maximum outer diameter of pod body/mm	89.42
Length of pod body/mm	402.4

2.2 Computational domain and mesh division

When the podded propulsor of the cruise ship runs, the watershed where it is located can be regarded as infinite. In this case, the influence of boundary conditions on the calculation results can be avoided by setting the calculation model to be infinite as well. However, a too-large watershed will significantly increase the calculation amount, so delineating a watershed within the allowable error range is recommended to balance calculation accuracy and calculation efficiency.

The computational domain of the podded propulsor is shown in Fig. 2. When the water in the watershed flows from the inlet to the outlet at a certain velocity, the podded propulsor can be regarded as moving forward in the water for further simulation of the motion state of the propulsor as the flow of the water is relative motion. In this paper, two computational domains of cylindrical shape are divided: a static domain with a larger diameter and a rotating domain with a smaller diameter. The static domain consists of the rotating domain, the strut, the pod body, and the fin. Although these components do not rotate in the computational domain, the propeller will rotate in the rotating domain. The intersection of the propeller disk and the centerline of the propeller shaft is taken as the coordinate origin, and the diameter D of the propeller is taken as the measurement unit of each computational domain. The diameter of the static domain is set to be 7D. The distance from the inlet to the propeller center is 5D, the distance from the outlet to the propeller center is 8D, and the length of the whole static domain is thus 13D. The diameter and length of the rotating domain are set to be 1.1D and 0.375D, respectively.

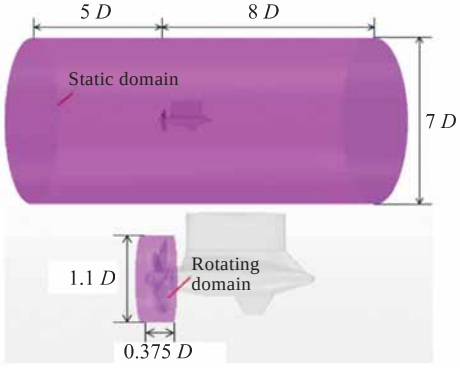

Fig. 2 Computational domain of podded propulsor

After the computational domain is determined, the Boolean subtraction operation can be applied to the rotating domain and the static domain, respectively, to obtain the rotating domain body and the static domain body. As the fluid flow near the propeller is complex, and the meshes in the rotating domain body have a great influence on the accuracy of the calculation results, the meshes in the rotating domain need to be densified. In contrast, the fluid flow in the relatively large static domain is simpler, and the mesh size can therefore be increased to a proper extent to reduce the number of meshes and thereby improve the computational efficiency. In addition to the body meshes divided, the surface meshes on the propeller blade and each interface, as well as the blade edge meshes, also need to be divided and locally densified. The mesh independence of the model is tested by controlling the global scale, changing the mesh setting parameters, and using the average relative error (that is, the average of the relative error between the simulation value and the experimental value under each advance coefficient) as the measurement standard. The results are shown in Fig. 3.

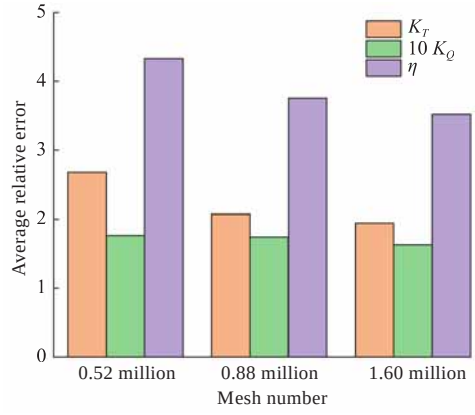

Fig. 3 Comparison of calculation results under different mesh numbers

Fig. 3 shows that the average relative errors of the thrust coefficient K_T, the torque coefficient $10K_Q$, and the open water efficiency η of the propel-

ler all decrease as the mesh number increases. When the mesh number increases from 0.88 million to 1.60 million, the calculated average relative errors of K_T, $10K_Q$, η are 4.8%, 4.4%, 4.5%, respectively, while the change rate of the actual simulation results is within 2%. Therefore, the mesh number is finally determined to be 0.88 million, in which the mesh numbers of the static domain and the rotating domain are 0.59 million and 0.29 million, respectively. The mesh division of the computational domain, the podded propulsor model, and the propeller surface is presented in Fig. 4.

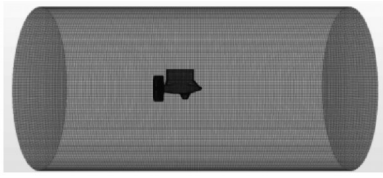

(a) Whole computational domain

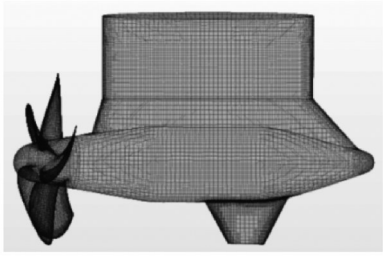

(b) Podded propulsor

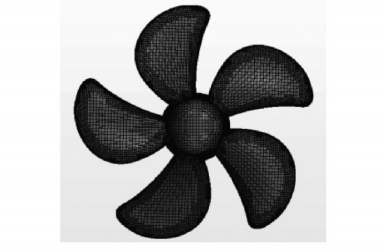

(c) Propeller surface

Fig. 4 Mesh division of computational domain, propulsor, and propeller

2.3 Setting of boundary conditions and calculation parameters

Since the velocity is constant and the pressure gradient is zero at the inlet of the static domain, the inlet is set as the velocity inlet. At the outlet of the static domain, the velocity and pressure gradient at the boundary are both zero since the fluid is fully developed. For calculation convenience, this paper sets the outer surface of the static domain as a symmetry plane. For the fluid in the rotating domain, the multiple reference frame motion model is used for calculation. When the fluid rotates, the propeller rotates with the x-axis as its rotation axis. The propeller wall of the podded propulsor is a slip wall, and the velocity of the fluid relative to the blades is zero. In contrast, the walls of other components are non-slip walls. The setting of boundary conditions and calculation parameters is shown in Table 2.

Table 2 Setting of boundary conditions and calculation parameters

Boundary conditions and calculation parameters	Definition or value
Far-field	Symmetry plane
Inlet of the static domain	Velocity inlet
Outlet of the static domain	Pressure outlet
Velocity amplitude	Field function VA
Solver	Segregated solver
Maximum propeller speed/(r·min^{-1})	898
Turbulence model	Realizable k-ε turbulence model
Fluid motion model	Multiple reference frame model
Pressure-velocity field coupling	SIMPLE algorithm
Inlet velocity	Field function VA
Turbulent kinetic energy	Fist-order upwind scheme
Turbulent dissipation rate	Fist-order upwind scheme

2.4 Experimental verification

In this paper, a test model of the podded propulsor (Fig. 5) is constructed according to the parameters in Table 1, and the open water performance of the propulsor is tested in the deepwater towing tank of the Shanghai Ship and Shipping Research Institute. The propulsor pod body is installed under the Z-type autonavigator, and its power is transmitted to the horizontal drive shaft through the vertical drive shaft in the autonavigator. Gear transmission is employed between the two shafts. The horizontal drive shaft installed in the pod body is connected to the test propeller, and the immersion depth of its horizontal axis is larger than 1.5D. The thrust of the whole podded propulsion unit can be obtained by connecting the vertical axis of the autonavigator to the six-component balance. The thrust axis of the propeller is equipped with a high-precision dynamometer to measure the thrust and torque of the propeller. In addition, a wave suppression plate is

Fig. 5 Model of podded propulsor and assembly state

also placed between the pod body and the autonavigator.

When the open water test is carried out, the thrust T and torque Q of the propeller at each advance speed are tested by the dynamometer, and the open water performance coefficient of the propeller can be obtained through conversion.

$$\begin{cases} J = \dfrac{V}{ND} \\ K_T = \dfrac{T}{\rho N^2 D^4} \\ K_Q = \dfrac{Q}{\rho N^2 D^5} \\ \eta = \dfrac{J}{2\pi}\dfrac{K_T}{K_Q} \end{cases} \tag{7}$$

where J is the advance coefficient; V is the inflow velocity; N is the propeller speed.

The advance coefficient J is within the range of 0.05−0.85. The comparison results of the open water performance coefficient of the propeller under different advance coefficients are shown in Fig. 6, where the subscripts of sim and test represent the simulation result and test result, respectively. According to Fig. 6, the errors in the propeller's thrust coefficient K_T and torque coefficient K_Q are small, with a maximum of 5.7%. The simulation value of the propeller's efficiency η agrees well with its experimental value under a low advance speed. Nevertheless, the relative error between them increases as the advance coefficient increases and exceeds 5% when the advance coefficient is over 0.7. The reason is that the thrust coefficient and the torque coefficient are both small under a high advance speed, and the relative error in the efficiency calculated is consequently amplified. Overall, the proposed simulation method achieves high accuracy and thus can meet the performance simulation requirements of the podded propulsor.

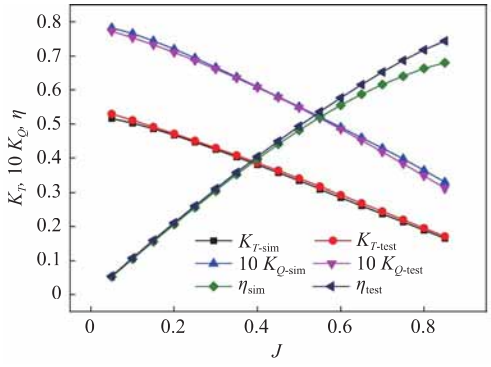

Fig. 6 Comparison between simulation results and test results of propeller's open water performance

3 Hydrodynamic performance of podded propulsor

3.1 Characteristic analysis of contours

In this section, the hydrodynamic performance of the podded propulsor is further analyzed on the basis of the pressure contours, velocity distribution contour, and flow-field velocity vector contour of the propulsor when the advance coefficient J = 0.7.

The pressure distribution on the propeller is shown in Fig. 7. Regarding the pressure distribution on the blade back in the left figure, blue areas can be observed at the leading edges, and the color in the middle areas of the leading edges is the deepest. The blue areas represent negative pressure regions, which indicate that the leading edges are under suction, and the maximum suction is located in the middle areas of the leading edges. The color from the leading edge to the trailing edge gradually transits from blue to yellowish-green, indicating that the suction gradually decreases from the leading edge to the trailing edge, and most area on the back of each blade is a suction surface. The pressure contour of the blade surface in the right part of Fig. 7 shows that yellow-orange areas are distributed at the leading edges of the blades, and the color is the darkest in the rear part near the blade root. The yellow-orange color represents positive pressure areas and thus indicates that the leading edges of the blades are under pressure and provide the forward thrust for the podded propulsor, with the maximum pressure located in the rear of the leading edges near the blade roots. The most area on the blade surface is under pressure, which gradually decreases from the leading edge to the trailing edge. In summary, the thrust of the podded propulsor is mainly generated by the blades' leading edges. Moreover, the blade surfaces are pressure surfaces, and the blade backs are suction surfaces.

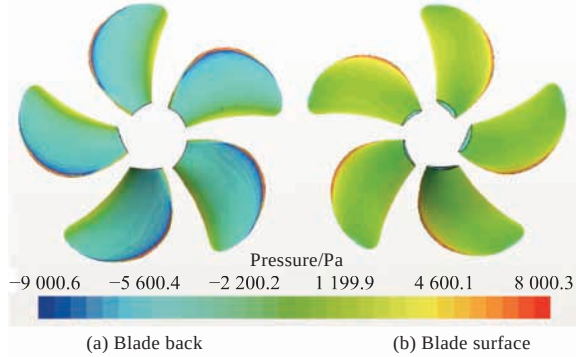

Fig. 7 Pressure contours of blades

Fig. 8 shows the pressure distribution on the surfaces of the pod body. In the figure, the forces acting on the pod body, strut, and fin surfaces are almost all positive pressure, but a small number of blue areas are also observed at the very front and very end of the fin. This indicates that suction is generated as well, which may be caused by the wake effect. The pressure distribution on the two sides of the pod body is basically balanced, while that on the two sides of the strut is not symmetrical. Specifically, the very front area on the left side of the strut is under positive pressure, whereas the very front area on the right side of the strut is under negative pressure. Furthermore, the negative pressure area at the rear of the left side of the strut is significantly larger than that on the right side, and the pressure difference between the two sides is likely caused by the different velocities of the wake generated by the rotation of the propeller when it is guided to the rear of the two sides of the strut. Overall, the pod body, the strut, and the fin provide essentially no thrust but resistance.

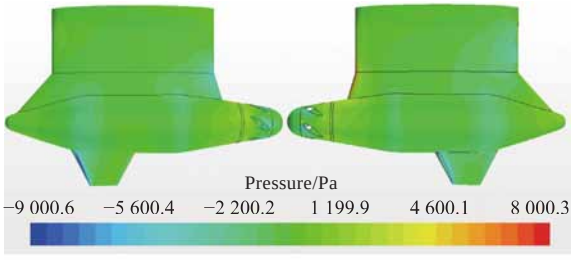

(a) Rear view (b) Front view

Fig. 8 Pressure contours of pod surfaces

Fig. 9 and Fig. 10 present the distribution of surface velocity and flow-field velocity vectors of the podded propulsor, respectively. In the two figures, the velocity is the largest at the propeller's blade tips and gradually decreases from the blade tips to the blade roots, while the velocities of the strut, the pod body, and the fin are small relative to the blades. This result is confirmed by the above pressure distribution and vice versa.

3.2 Influence analysis of pod body geometry

To further study the influence of the pod body geometry on the hydrodynamic performance of the whole propulsor, this paper takes the model in Table 1 as the prototype, adjusts the length-to-diameter ratio (i.e., the ratio of the length of the pod body to the maximum diameter of the pod body) of the pod to 1.2 and 0.8 times of the prototype, respectively,

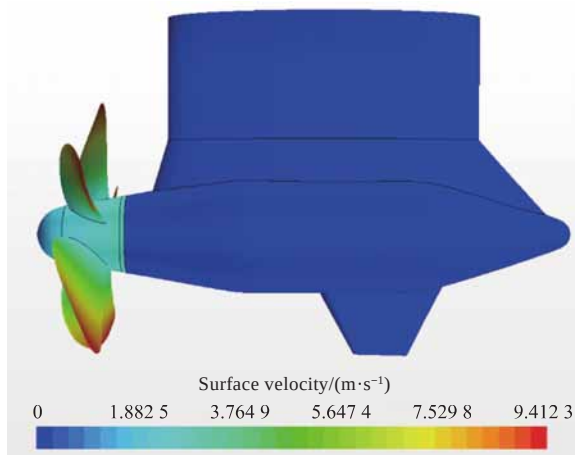

Fig. 9 Contours of surface velocity distribution

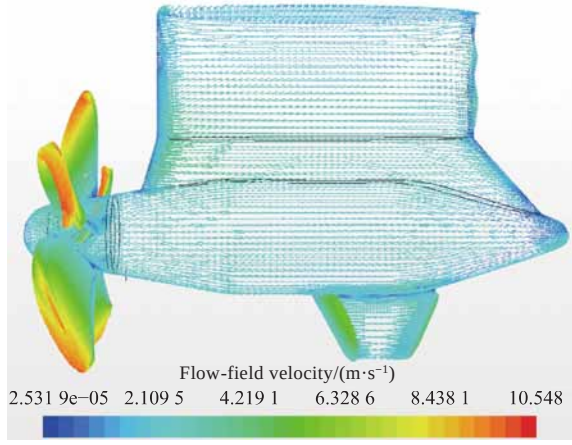

Fig. 10 Flow-field velocity vector contour

and keeps the propeller's parameters unchanged. The simulation results of the open water performance of the propulsor obtained are shown in Fig. 11. When the pod body geometry of the podded propulsor changes, the thrust coefficient K_T, torque coefficient K_Q, and open water efficiency η of the podded propulsor all change slightly, so studying the open water performance of the podded propulsor from the perspective of the length-to-diameter ratio of the pod body is of limited potential. Nevertheless, the pod body geometry changes the propulsor resistance greatly, and further research can thus be carried out from the perspective of reducing the resistance of the podded propulsor.

3.3 Influence analysis of disk ratio of propeller

Since the change in the disk ratio of the propeller leads to changes in a series of parameters, such as the chord length and blade thickness, the disk ratio of the propeller is a common design parameter in the design optimization of podded propulsors. In this section, the model in Table 1 is taken as the prototype (its disk ratio is 0.67). With the other parame-

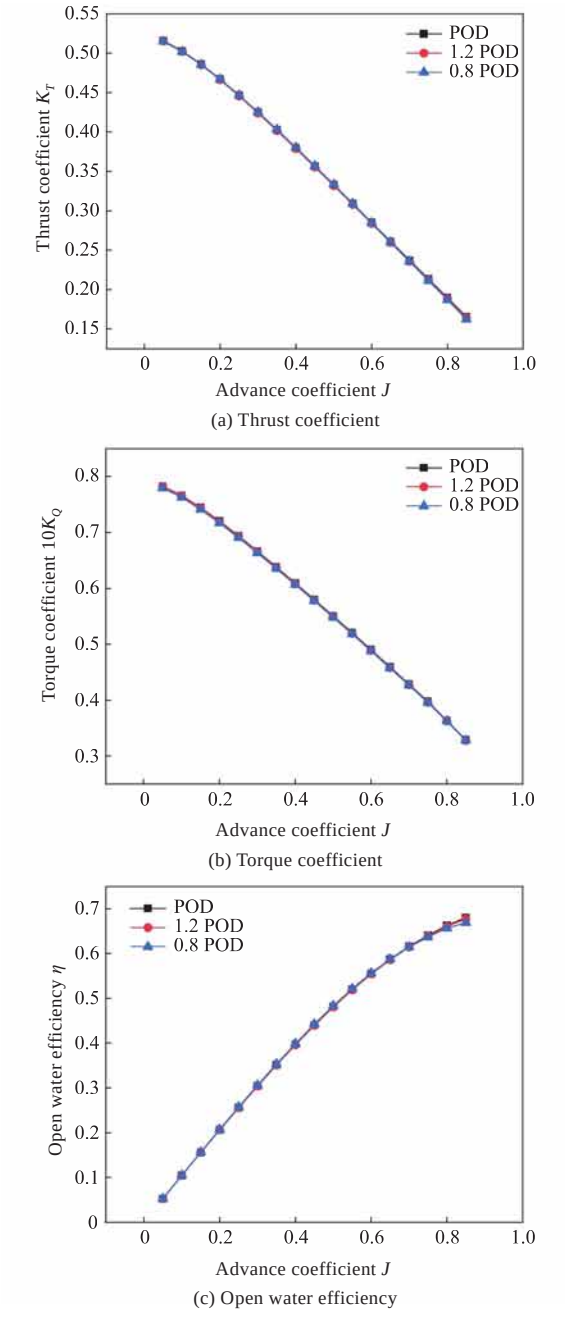

Fig. 11 Influence of pod body geometry on propulsor's open water performance

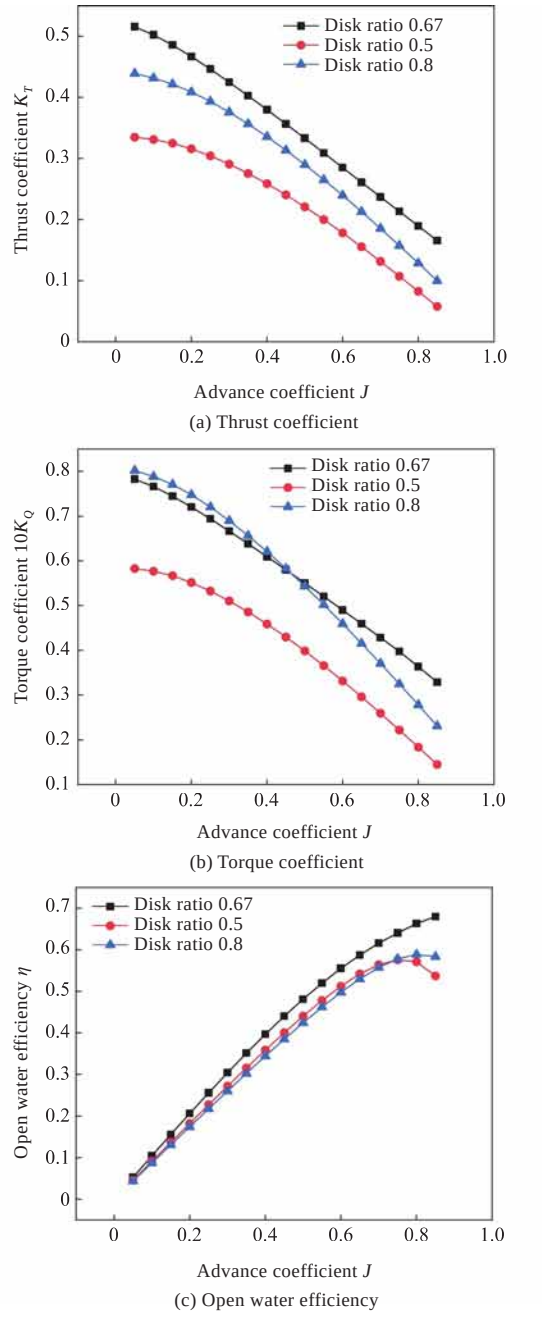

Fig. 12 Influence of disk ratio of propeller on propulsor's open water performance

ters unchanged, the disk ratio of the propeller is changed alone to 0.5 and 0.8, respectively, and the hydrodynamic performance of the podded propulsor is then calculated. The simulation results are shown in Fig. 12.

As can be seen from Fig. 12, the thrust coefficient and open water efficiency of the podded propulsor both increase first and then decrease as the disk ratio increases under a constant advance coefficient. When the advance coefficient is smaller than 0.75, the podded propulsor with a disk ratio of 0.8 has the lowest open water efficiency. Regarding the torque coefficient, a larger disk ratio corresponds to a larger torque coefficient when the advance coefficient is smaller than 0.45. When the advance coefficient is larger than 0.45, the torque coefficient increases first and then decreases with the increase in the disk ratio. Therefore, a larger disk ratio of the propeller is not necessarily better for the optimization of the hydrodynamic performance of the podded propulsor, and an appropriate disk ratio should be selected according to the specific application requirements.

3.4 Influence analysis of propeller blade number

Generally speaking, a smaller propeller blade number results in higher propulsion efficiency.

However, the influences of different propeller blade numbers on the open water performance of the podded propulsor at different advance speeds are also different. Therefore, this section takes the model in Table 1 as the prototype, merely changes the propeller blade number (4, 5, and 6 blades) of the podded propulsor, and comparatively analyzes the influences of different blade numbers on the hydrodynamic performance of the podded propulsor. The simulation results are shown in Fig. 13. This figure reveals that the thrust coefficient, torque coefficient, and open water efficiency of the podded propulsor all increase first and then decrease with the increase in the propeller blade number under a constant advance coefficient. However, the change in the propeller blade number has a small influence on the open water efficiency of the podded propulsor under a low advance coefficient. With the increase in the advance coefficient, the influence of the blade number on the open water efficiency also increases gradually.

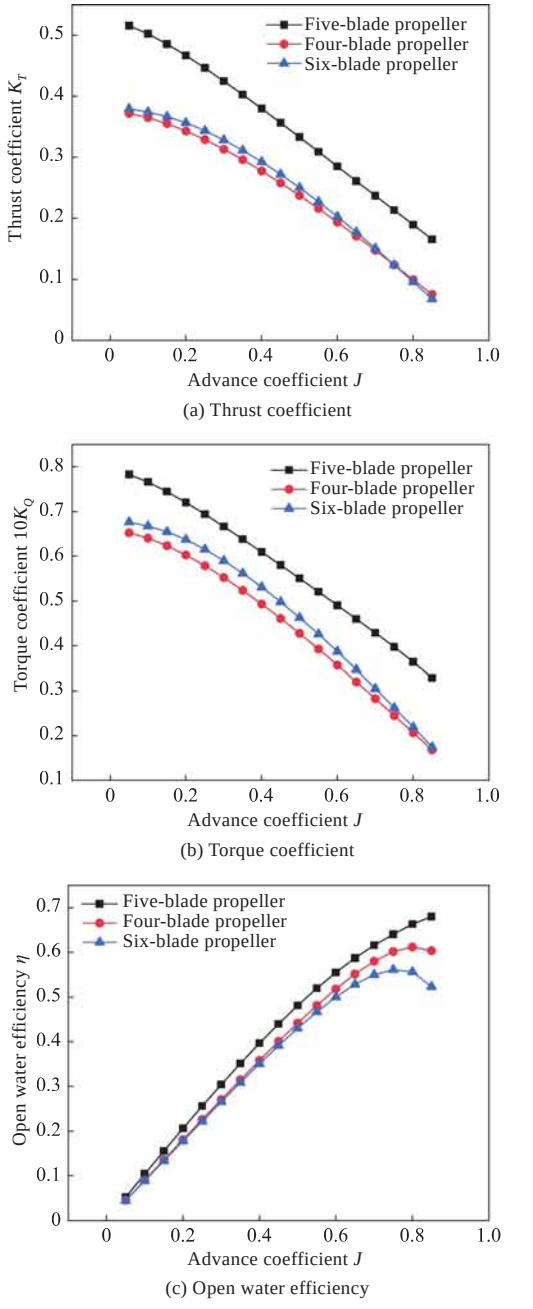

Fig. 13 Effect of blade number on open water performance of the propulsor

4 Conclusions

This paper investigates the influences of the structural parameters of the podded propulsor on its open water performance and mainly obtains the following conclusions.

1) The results of open water performance tests of the propulsor in the deepwater towing tank show that the hydrodynamic characteristic simulation method for podded propulsors based on the RANS theory offers high accuracy.

2) The propeller blade backs are suction surfaces, and its blade surfaces are pressure surfaces, with the pressure and suction both gradually reducing from the leading edges to the trailing edges. The pod, the strut, and the fin basically do not provide thrust. The pressure on the two sides of the pod is basically balanced, but that on the two sides of the strut is not symmetrically distributed.

3) The length-to-diameter ratio of the pod body has a small influence on the open water performance of the podded propulsor, but it changes the resistance of the propulsor greatly. The thrust coefficient and open water efficiency of the podded propulsor both increase first and then decrease with the increase in the disk ratio of the propeller, while the torque coefficient increases only in a certain range and increases first and then decreases when it exceeds the range. When the blade number increases, the thrust coefficient, torque coefficient, and open water efficiency of the propulsor all increase first and then decrease, and the blade number has a small influence on the open water efficiency of the podded propulsor under a low advance coefficient. Its influence gradually increases as the advance coefficient rises.

References

[1] HAN Y, ZHANG Z, SHEN X R. Research on open water performance of POD propeller[C]//The Chinese Society of Naval Architects and Marine Engineers. Proceedings of 2009 Academic Conference on Ship Hydrodynamics and the 30th Anniversary of China's Entry into ITTC. Beijing: The Chinese Society of Naval Architects and Marine Engineers, 2010: 120−127 (in

Chinese).
[2] HANSEN J F, WENDT F. History and state of the art in commercial electric ship propulsion, integrated power systems, and future trends [J]. Proceedings of the IEEE, 2015, 103 (12): 2229−2242.
[3] ISLAM M F, VEITCE B, LIU P. Experimental research on marine podded propulsors [J]. Journal of Naval Architecture and Marine Engineering, 2007, 4 (2): 57−71.
[4] HE W, CHEN K Q, LI Z R. Experimental research on hydrodynamics of tandem podded propulsor in azimuthing conditions [J]. Journal of Huazhong University of Science and Technology (Natural Science Edition), 2015, 43 (1): 107−111 (in Chinese).
[5] ISLAM M, AKINTURK A, VEITCH B. Performance aspects of podded propulsor in dynamic operating conditions [J]. International Shipbuilding Progress, 2016, 62 (3/4): 139−160.
[6] ZHAO D G, GUO C Y, WU T C, et al. Hydrodynamic interactions between bracket and propeller of podded propulsor based on particle image velocimetry test [J]. Water, 2019, 11 (6): 1142.
[7] FENG P Y, WU Y S, FENG Y, et al. An experimental prediction method of power increases of a cruise ship with podded propulsion in waves [J]. Chinese Journal of Ship Research, 2020, 15 (5): 11−16 (in Chinese).
[8] CHENG B H, DEAN J S, MILLER R W, et al. Hydro dynamic evaluation of hull forms with podded propulsors [J]. Naval Engineers Journal, 1989,101 (3): 197−206.
[9] TASKAR B, STEEN S, ERIKSSON J. Effect of waves on cavitation and pressure pulses of a tanker with twin podded propulsion [J]. Applied Ocean Research, 2017, 65: 206−218.
[10] BAL A, GÜNER M. Performance analysis of podded propulsors [J]. Ocean Engineering, 2009, 36 (8): 556−563.
[11] YE J M, XIONG Y. Prediction of podded propeller cavitation using an unsteady surface panel method [J]. Journal of Hydrodynamics,Ser. B,2008,20(6):790−796.
[12] SHAMSI R, GHASSEMI H, MOLYNEUX D, et al. Numerical hydrodynamic evaluation of propeller (with hub taper) and podded drive in azimuthing conditions [J]. Ocean Engineering, 2014, 76: 121−135.
[13] ZHU Z C, XIONG Y. Research on the CFD prediction method of hydrodynamic performance of tandem type podded propulsor [J]. Ship Science and Technology, 2016, 38 (3): 14−19 (in Chinese).
[14] ZHANG Y X, WU X P, ZHOU Z Y, et al. A numerical study on the interaction between forward and aft propellers of hybrid CRP pod propulsion systems [J]. Ocean Engineering, 2019, 186: 106084.
[15] YAO Z Q, XU Z R, LING H J, et al. Analysis of hydrodynamic characteristics of pull podded thruster [J]. Ship Science and Technology, 2020, 42 (5): 44−49 (in Chinese).
[16] WANG G B, XIE Y H, XU S J, et al. Analysis and comparison of different turbulence models in the computation of propeller's hydrodynamic performance [J]. Journal of Zhejiang Ocean University (Natural Science), 2014, 33 (6): 526−530 (in Chinese).
[17] DONG X Q. Numerical study of the hydrodynamic performance of podded propulsor [D]. Shanghai: Shanghai Jiao Tong University, 2013.

邮轮吊舱推进器水动力性能仿真研究

聂远哲[1],欧阳武[*1,2],李高强[1],张聪[1,2],周新聪[1,2]
1 武汉理工大学 交通与物流工程学院,湖北 武汉 430063
2 国家水运安全工程技术研究中心 可靠性工程研究所,湖北 武汉 430063

摘　要:[**目的**]为研究邮轮吊舱推进器组合式水力组件与其敞水性能间的相互映射关系,提出基于雷诺平均纳维—斯托克斯(RANS)方程的吊舱推进器水动力性能预报方法。[**方法**]以邮轮吊舱推进器缩比模型为研究对象,在深水拖曳水池中开展推进器敞水性能试验,对预报方法进行精度验证。通过仿真计算,分析吊舱推进器舱体形状、螺旋桨盘面比和桨叶数对吊舱推进器水动力性能的影响规律。[**结果**]结果表明:舱体形状对推进器敞水性能的影响较小;提高螺旋桨盘面比时,推进器的推力系数和敞水效率均先增后减,而转矩系数则在一定范围内随之增加;增加螺旋桨叶数时,推进器的推力系数、转矩系数和敞水效率均先增加后减小,而桨叶数对低进速系数下吊舱推进器敞水效率的影响较小。[**结论**]研究成果可为吊舱推进器的优化设计提供参考。

关键词:邮轮;吊舱推进器;水动力性能;计算流体动力学(CFD);优化设计